A Density Functional Study of Chain Growing and Chain Terminating Steps in Olefin Polymerization by Metallocene and Constrained Geometry Catalysts

T. K. Woo,[†,‡] L. Fan,[†] and T. Ziegler*[,‡]

Novacor Research & Technology Corporation, Calgary, Alberta, Canada T2E 7K7, and Department of Chemistry, University of Calgary, Calgary, Alberta, Canada T2N 1N4

Received November 29, 1993[⊗]

Nonlocal density functional (DF) calculations have been carried out on the insertion of ethylene into the metal–CH_3 bond of the Kaminsky type metallocenes: $Cp_2ZrCH_3^+$ (**2a**), $(SiH_2Cp_2)ZrCH_3^+$ (**3a**), Cp_2ScCH_3 (**4a**), and the constrained geometry catalyst (CGC) $(SiH_2(Cp)NH)ZrCH_3^+$ (**5a**). The objective has been to study the energy profile for the insertion involving **2a** and how it is modified by introducing the silane bridge in **3a**, replacing one Cp with NH in **5** or switching to the neutral system **4a**. The DF calculations reveal that the insertion into the bis-Cp systems proceeds with a modest barrier of 3, 4, and 14 kJ/mol for **2**–**4**, respectively. This barrier is marginally influenced by going from the charged species $Cp_2ZrCH_3^+$ (**2a**) to the neutral system Cp_2ScCH_3 (**4a**) and is unchanged in going from the unbridged system $Cp_2ZrCH_3^+$ (**2a**) to the silane bridged system (**3a**). The systems **2a**, **3a**, and **4a** all form a π-complex with a very shallow minimum at the beginning of the insertion process. The insertion process for the zirconium CGC (**5a**) exhibits a clear activation barrier and a pronounced minimum for the π-complex. The deeper potential well of the π-complex in **5a** compared to **2a**, **3a**, and **4a** can be related to a reduction in the steric interaction between ethylene and the ligands on the metal center as one Cp ring is replaced by a NH ligand. The higher barrier in the case of **5a** is a consequence of the stable π-complex which has to be abandoned in order to proceed to the insertion product. Calculations have also been carried out on two chain terminating steps. The first step involved β-hydride elimination. It is concluded that this process is unfavorable for early transition metal centers with an endothermicity of 176 kJ/mol. The second step is concerned with the activation of an ethylene C–H bond by the metallocene to form an alkane and a vinylzirconocene. It is concluded that this process is viable as a chain terminating step.

I. Introduction

Metallocenes of early transition metals and f-block elements are currently under intense investigation[1] as alternative catalysts to the traditional heterogeneous Ziegler–Natta systems in olefin polymerization. Of particular promise has been the cationic metallocenes of group-4 elements first developed by Kaminsky and Brintziner.[1a] The cationic catalysts are often generated from neutral dichlorometallocenes of group-4 elements by the reaction with a cocatalyst such as methylaluminoxane (MAO) according to eq 1. The polymer is formed in subsequent reactions between olefin and the cationic alkyl species according to eq 2.

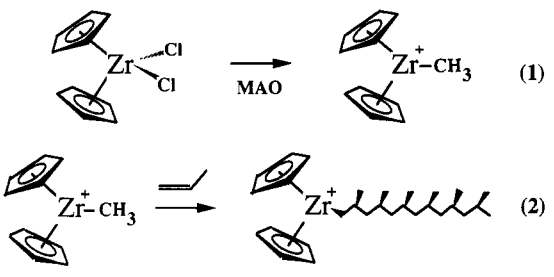

The Cossee scheme[2] is the most widely accepted mechanism for polymerization of olefins by heterogeneous Ziegler–Natta systems as well as the homogeneous metallocene catalysts. This mechanism is shown for metallocene systems in eq 3. The active species **1a** of eq 3

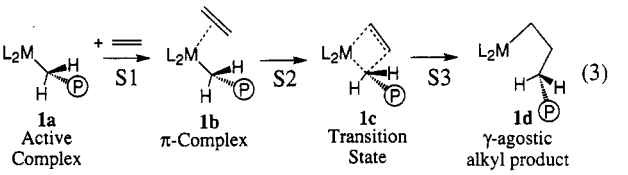

possesses a vacant coordination site, and for the group-4 based systems **1a** represents the alkylated cationic met-

(1) (a) Kaminsky, W.; Kulper, K.; Brintzinger, H. H.; Wild, F. R. W. P. *Angew. Chem. Int., Ed. Engl.* **1992**, *31*, 1347. (b) Jordan, R. F.; LaPoint, R. E.; Baenziger, N. C.; Hinch, G. D. *Organometallics* **1990**, *9*, 1539. (c) Borkowsky, S. L.; Jordan, R. F.; Hinch, G. D. *Organometallics* **1991**, *10*, 1268. (d) Hlatky, G. G.; Eckman, R. R.; Turner, H. W. *Organometallics* **1992**, *11*, 1413. (e) Ewen, J. A.; Elder, M. J.; Jones, R. L.; Haspeslagh, L.; Atwood, J. L.; Bott, S. G.; Robinson, K. *Makromol. Chem., Macromol. Symp.* **1991**, *48/48*, 253. (f) Zambelli, A.; Long, P.; Grassi, A. *Macromolecules* **1989**, *22*, 2186. (g) Eshuis, J. J.; Tan, Y. Y.; Meetsma, A.; Teuben, J. H. *Organometallics* **1992**, *11*, 362. (h) Yang, X.; Stern, C. L.; Marks, T. J. *J. Am. Chem. Soc.* **1991**, *113*, 3623. (i) Horton, A. D.; Orpen, A. G. *Organometallics* **1991**, *10*, 3910. (j) Chien, J. C. W.; Tsai, W. M.; Rausch, M. D. *J. Am. Chem. Soc.* **1991**, *113*, 8570. (k) Eisch, J. J.; Caldwell, K. R.; Werner, S.; Krüger, C. *Organometallics* **1991**, *10*, 3417. (l) Stevens, J. C.; Timmers, F. J.; Wilson, D. R.; Schmidt, G. F.; Nicklas, P. N.; Rosen, R. K.; Knight, G. W.; Lai, S. Eur. Pat. Appl. EP-416-815-A2, March 13, 1991 (Dow). (m) Canich, J. A. PCT Appl. WO 91.04257, April 4, 1991 (Exxon). (n) Kaminsky, W.; Steiger, R. *Polyhedron* **1988**, *7*, 2375.

(2) (a) Cossee, P. *J. Catal.* **1964**, *3*, 80. (b) Arlman, E. J.; Cossee, P. *J. Catal.* **1964**, *3*, 99.

† Novacor Research and Technology Corp.
‡ University of Calgary.
⊗ Abstract published in *Advance ACS Abstracts*, April 1, 1994.

0276-7333/94/2313-2252$04.50/0

allocene. The first step, S1, of the insertion process involves the complexation of olefin to form a π-complex, **1b**. In the second step, S2, the olefin inserts into the metal–carbon bond to form a four-membered cyclic transition state, **1c**, which reacts further in S3 to form the longer chain **1d**. The newly formed species, **1d**, possesses a vacant coordination site where the M–C bond formerly was in **1a**. It can thus serve as the starting point for the next insertion step.

For the homogeneous group-4 catalysts the exact nature of the active species is a subject of debate. The current belief[3] is that the active species is a cationic complex such as Cp_2ZrR^+. Jordan and co-workers have detected that the benzyl species $Cp_2Zr(CH_2Ph)^+$ catalyzes ethylene polymerization.[3c] The role of the cocatalyst, usually MAO, is even less understood. It is thought that the cocatalyst may act only to generate the active species and possible clean up contaminants. On the other hand, it may play a more fundamental role such as assisting in the insertion of each monomer unit.

The objective of the present study has been to carry out theoretical calculations on olefin polymerization catalyzed by group-4 metallocenes. The calculations will be based on density functional theory[4] (DFT). In this investigation we are adopting the model of an unassociated cationic active species of the olefin polymerization, eq 3. The active role of the MAO as well as the influence of the solvent is neglected for practical reasons and for the reason that the exact structure of the MAO cocatalyst in these systems is unknown.[1n]

We shall consider the active species $Cp_2ZrCH_3^+$, **2a**, SiH_2-$Cp_2ZrCH_3^+$, **3a**, Cp_2Sc–CH_3, **4a**, and the silylamido bridged system, $SiH_2NHZrCH_3^+$, **5a**. The species **2a** and **3a** model

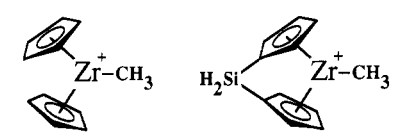

2a **3a**

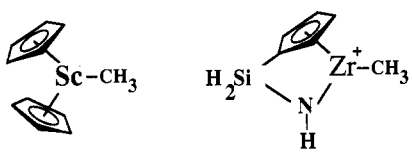

4a **5a**

the bis-Cp Kaminsky type catalysts[1a] with and without a silane bridge, whereas **5a** is a zirconium derivative of the constrained geometry catalysts (CGC) used in polymerization systems recently patented by Dow[11] and Exxon.[1m] Our objective has been to study the first insertion step in the polymerization process after the active methyl species has been formed from the chlorometallocenes according to eq 1. We shall trace the energy profile for the insertion of ethylene into the Zr–CH_3 bond of **2a**. This will provide us with information about the electronic factors of importance for the insertion. We shall further trace the profiles for the insertion processes involving **3a**, **4a**, and **5a**. Such a comparative study will provide information

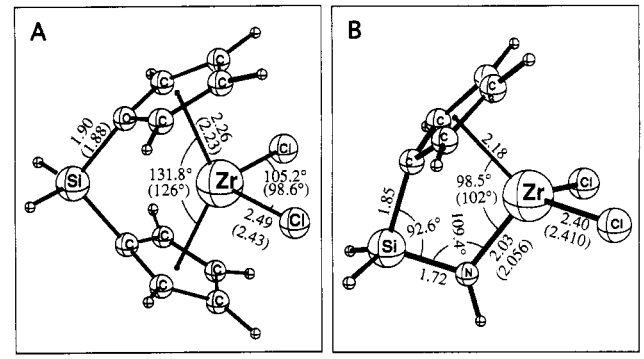

Figure 1. Optimized structures of dichloro metallocenes: (A) $SiH_2Cp_2ZrCl_2$; (B) $SiH_2NHZrCl_2$.

about how the profile is changed by introducing the silane bridge in **3a**, replacing Cp with NH in **5a**, or switching to the neutral system **4a**. Later studies will deal with the steric influence of the polymer in Figure 1 by considering ethylene insertion into metal–propyl bonds.

Many molecular orbital studies have been carried out on the insertion of ethylene into the metal–hydrogen and metal–alkyl bonds.[5] The theoretical work on Kaminsky type catalysts has been initiated by Castonguay and Rappe[5c] as well as Koga, Morokuma, and co-workers.[5a,b] However, none of the previous studies have modeled the half-sandwich CGC catalyst **5** or made comparisons between a series of active species. In addition, previous studies have either used low levels of theory, Hartree–Fock geometries, and energies based on second order Møller–Plesset (MP2) or simplified the model even further by, for example, replacing Cp rings with Cl atoms.[5b,c] The results presented here have already been presented in preliminary form.[6]

The insertion process of eq 3 constitutes the productive chain growing step in olefin polymerization. We shall compare the profile of this reaction with the energy profiles of two competing chain terminating steps in the last part of our study. The two steps are β-hydride elimination

$$L_2M\text{–}CH_2CH_2R \rightarrow L_2M\text{–}H + CH_2CHR \qquad (4)$$

and activation of a C–H bond in olefin

$$L_2M\text{–}R + C_2H_4 \rightarrow L_2M\text{–}C(H)CH_2 + RH \qquad (5)$$

The calculations in this part of the study will be carried out with Cp_2Zr^+ as the model metal fragment L_2M.

II. Computation Details

The reported density functional calculations were all carried out by utilizing the program system AMOL,

(3) (a) Gassman, P. G.; Callstrom, M. R. *J. Am. Chem. Soc.* **1987**, *109*, 7875. (b) Jordan, R. F.; Bajgur, C. S.; Willett, R.; Scott, B. *J. Am. Chem. Soc.* **1986**, *108*, 7410. (c) Alelynuas, Y. W.; Jordan, R. F.; Echols, S. F.; Borkowsky, S. L.; Bradley, P. K. *Organometallics* **1991**, *10*, 1406.

(4) Ziegler, T. *Chem. Rev.* **1991**, *91*, 651.

(5) (a) Kawamura-Kuribayashi, H.; Koga, N.; Morokuma, K. *J. Am. Chem. Soc.* **1992**, *114*, 8687. (b) Kawamura-Kuribayashi, H.; Koga, N.; Morokuma, K. *J. Am. Chem. Soc.* **1992**, *114*, 2359. (c) Castonguay, L. A.; Rappe, A. K. *J. Am. Chem. Soc.* **1992**, *114*, 5832. (d) Lauer, J. W.; Hoffman, R. *J. Am. Chem. Soc.* **1976**, *98*, 1729. (e) Jolly, C. A.; Marynick, D. S. *J. Am. Chem. Soc.* **1989**, *111*, 7968. (f) Versluis, L.; Ziegler, T.; Fan, L. *Inorg. Chem.* **1990**, *29*, 4530. (g) Novaro, O.; Chow, S.; Magnouat, P. *J. Catal.* **1979**, *42*, 131. (h) Prosenc, M.; Janiak, C.; Brintzinger, H. *Organometallics* **1992**, *11*, 4036. (i) Hart, J. R.; Rappé, A. K. *J. Am. Chem. Soc.* **1993**, *115*, 6159. (j) Gleiter, R.; Hyla-Kryspin, I.; Niu, S.; Erkert, G. *Organometallics* **1993**, *12*, 3828. (k) Mohr, R.; Berke, H.; Erker, G. *Helv. Chim. Acta* **1993**, *76*, 1389.

(6) (a) Woo, T.; Fan, L.; Ziegler, T. *Organometallics* **1994**, *13*, 432. (b) International Symposium: 40 years of Ziegler Catalysts. Freiburg, Germany, September 1–3, 1993.

developed by Baerends *et al.*[7,8] and vectorized by Ravenek.[9] The numerical integration procedure applied for the calculations was developed by te Velde[10] *et al.* The geometry optimization procedure was based on the method developed by Versluis[11] and Ziegler. The electronic configurations of the molecular systems were described by an uncontracted triple-ζ STO basis set[12] on scandium for 3d, 4s, and 4p and an uncontracted triple-ζ STO basis set[12] on zirconium for 4s, 4p, 4d, 5s, and 5p. Double-ζ STO basis sets[12] were used for carbon (2s, 2p), hydrogen (1s), silicon (3s, 3p), and nitrogen (2s, 2p), augmented with a single 3d polarization function except for hydrogen where a 2p function was used. Polarization functions were not employed for the carbons and hydrogens on the Cp rings. The $1s^2 2s^2 2p^6 3s^2 3p^6 3d^{10}$ configuration on zirconium, the $1s^2 2s^2 2p^6$ configuration on scandium, and the $1s^2$ configuration on carbon and nitrogen as well as the $1s^2 2s^2$ configuration on silicon were assigned to the core and treated by the frozen-core approximation.[8] A set of auxiliary[13] s, p, d, f, and g STO functions, centered on all nuclei, was used in order to fit the molecular density and present Coulomb and exchange potentials accurately in each SCF cycle. Energy differences were calculated by including the local exchange-correlation potential by Vosko[14] *et. al.* with Becke's[15] nonlocal exchange corrections and Perdew's[16] nonlocal correlation correction. Geometries were optimized without including nonlocal corrections. The application of approximate density functional theory to organometallic chemistry has been reviewed recently.[17]

III. Chain Propagating Step

We shall begin our study of the olefin insertion process in eq 3 by a discussion of the optimized geometries for **2a**, **3a**, **4a**, and **5a** as well as the dichloro precursors to **3a** and **5a**. This discussion will be followed by a detailed examination of the three steps S1, S2, and S3 of eq 3 with **2a** as the catalyst. The results based on **2a** will finally be compared to the profiles obtained using **3a**, **4a**, and **5a**.

A. Optimized Structures of Precursors and Active Methyl Species. The optimized structure of $SiH_2Cp_2ZrCl_2$ is shown in Figure 1A. The structure was fully optimized within C_s symmetry constraints. Figure 1A displays the important geometric parameters with experimental values[18a] shown in parentheses. The agreement with experiment is in general good. It might be improved by employing a more extensive basis set on the Cp rings as well as nonlocal corrections in the geometry optimization. However, such an extension is not possible with the available computational resources.

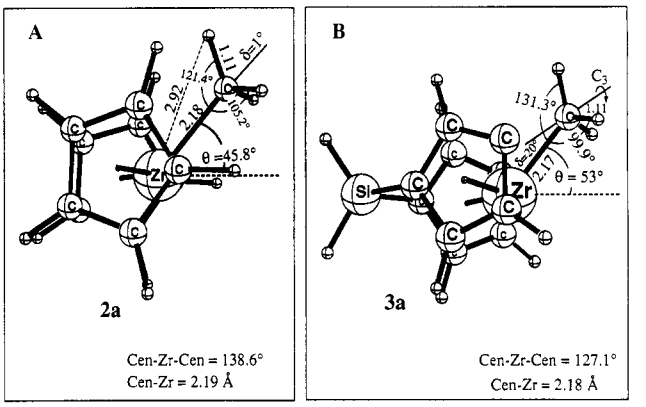

Figure 2. Optimized geometries for methylated metallocenes: (A) $Cp_2ZrCH_3^+$, **2a**; (B) $SiH_2Cp_2ZrCH_3^+$, **3a**. Some hydrogens have been omitted for clarity.

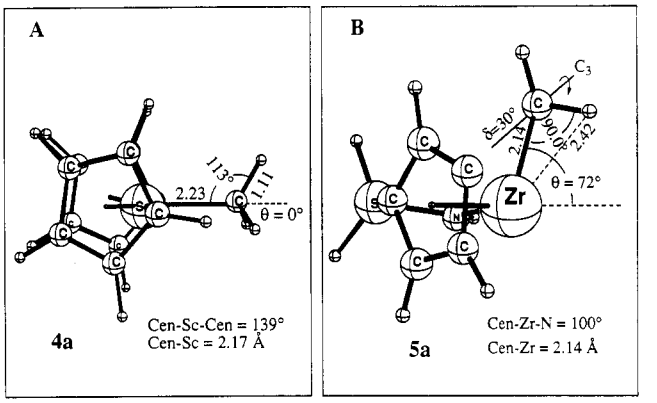

Figure 3. Optimized geometries for methylated Cp systems: (A) Cp_2ScCH_3, **4a**; (B) $SiH_2NHCpZrCH_3^+$, **5a**. Some hydrogens have been omitted for clarity.

The optimized geometry for $SiH_2CpNHZrCl_2$ is shown in Figure 1B, again with known experimental parameters shown in parentheses. This species is related to the constrained geometry catalyst $(SiH_2(NH)(Cp))ZrCH_3^+$, **5a**. The structure of $SiH_2CpNHZrCl_2$ was optimized fully in C_s symmetry, and the theoretical geometry is in excellent agreement with the experimental crystal structure.[18b]

The optimized geometries of $Cp_2ZrCH_3^+$, **2a**, and $SiH_2Cp_2ZrCH_3^+$, **3a**, are given in Figure 2 with those of Cp_2ScCH_3, **4a**, and $SiH_2NHCpZrCH_3^+$, **5a**, displayed in Figure 3. All degrees of freedom within C_s symmetry constraints were optimized at the LDA level for structures **2a**, **3a**, and **4a**. The CGC, **5a**, was fully optimized at the LDA level with no symmetry constraints.

The structures of **2a** and **3a** may be compared to the experimental "cation-like" X-ray structures of $[1,2\text{-}Me_2Cp]_2ZrCH_3^+ - CH_3B(C_5F_5)_3^-$ **6**,[19] and $[Me_5Cp]_2ZrCH_3^+ - CH_3B(C_5F_5)_3^-$, **7**.[20] In **6** and **7** the methyl fragment of the

(7) Baerends, E. J.; Ellis, D. E.; Ros, P. *Chem. Phys.* **1973**, *2*, 41.
(8) Baerends, E. J. Ph.D. Thesis, Vrije Universiteit, Amsterdam, 1975.
(9) Ravenek, W. In *Algorithms and Applications on Vector and Parallel Computers*; te Riele, H. J. J., Dekker, Th. J., van de Vorst, H. A., Eds.; Elsevier, Amsterdam, 1987.
(10) (a) Boerrigter, P. M.; te Velde, G.; Baerends, E. J. *Int. J. Quantum Chem.* **1988**, *33*, 87. (b) te Velde, G.; Baerends, E. J. *J. Comput. Phys.* **1992**, *99*, 84.
(11) Versluis, L.; Ziegler, T. *J. Chem. Phys.* **1988**, *88*, 322.
(12) (a) Snijders, G. J.; Baerends, E. J.; Vernooijs, P. *At. Nucl. Data Tables* **1982**, *26*, 483. (b) Vernooijs, P.; Snijders, G. J.; Baerends, E. J. Slater Type Basis Functions for the whole Periodic System. Internal Report, Free University of Amsterdam, The Netherlands, 1981.
(13) Krijn, J.; Baerends, E. J. Fit functions in the HFS-method. Internal Report (in Dutch), Free University of Amsterdam, The Netherlands, 1984.
(14) Vosko, S. H.; Wilk, L.; Nusair, M. *Can. J. Phys.* **1990**, *58*, 1200.
(15) Becke, A. D. *Phys. Rev.* **1988**, *A38*, 3098.
(16) Perdew, J. P. *Phys. Rev.* **1986**, *B33*, 8822; 1986, *B34*, 7406.
(17) (a) Ziegler, T. *J. Pure Appl. Chem.* **1991**, *63*, 873. (b) Ziegler, T.; Versluis, L. *Adv. Chem. Ser.* **1992**, *230*, 75. (c) Ziegler, T.; Tschinke, T. *ACS Symp. Ser.* **1990**, *428*, 277. (d) Ziegler, T.; Snijders, J. G.; Baerends, E. J. *ACS Symp. Ser.* **1989**, *383*, 322. (e) Ziegler, T.; Tschinke, V.; Versluis, L. *NATO ASI Ser.* **1986**, *C176*, 189. (f) Ziegler, T. *NATO ASI Ser.* **1992**, *C367*, 357. (g) Ziegler, T. *NATO ASI Ser.* **1992**, *C378*, 367.
(18) (a) Burger, P.; Hortmann, K.; Diebold, J.; Brintzinger, H. *J. Organomet. Chem.* **1991**, *417*, 9. The experimental crystal structure is of (R,S)-$(CH_3)_2Si(1\text{-}C_5H_2\text{-}2\text{-}CH_3\text{-}4\text{-}C_6H_5)_2ZrCl_2$. (b) Stevens, J. C. Metcon 93, Houston, May 26–28, 1993.
(19) Yang, X.; Stern, C. L.; Marks, T. J. *J. Am. Chem. Soc.* **1991**, *113*, 3623.
(20) Marks, T. J. Private communication of work in progress.

$CH_3B(C_5F_5)_3^-$ anion is weakly coordinated with the zirconium center. Of the two complexes, **7** best models the free cation because the fully methylated Cp ring pushes the anion further away from the Zr center than in **6**. The optimized geometries of **2a** and **3a** are in reasonable agreement with structures **6** and **7**. The optimized zirconium methyl-carbon distance, $Zr-C_{Me}$, of 2.18 Å is 0.04 Å shorter than the experimental value of 2.22 Å in **7**. Structure **6** which possesses a $Zr-C_{Me}$ distance of 2.25 Å reveals that the $Zr-C_{Me}$ distance decreases as the counteranion is less associated with the cationic zirconocene. Thus, the optimized value of 2.18 Å is a reasonable estimate of the $Zr-C_{Me}$ distance in the free cation. At the same time, LDA geometries tend to underestimate bond distances. The $Zr-C_{Me}$ distance of 2.17 Å in **3a** is also reasonable. The average Zr–C(Cp) distance of 2.50 Å in **2a** and 2.49 Å in **3a** is in good agreement with the experimental value of 2.525 Å in **6**. For the unbridged zirconocene, **2a**, the optimized Cp centroid–Zr–centroid angle of 138.6° is also in good agreement with the experimental value of 132.5° observed in **6**. The most notable feature of **2a**, **3a**, and **5a** is the direction of the methyl group. The "bent sandwich" configuration is in agreement with experimental structures[19] and work by Hoffmann[5d] *et al.* who predict that the optimal θ angle is 65° when only electronic factors are considered. On the other hand, the structures contradict the "straight" Hartree-Fock optimized structures of Morokuma and co-workers.[5a,b] It should be noted that the bent and straight geometries were found to differ by only 1 kcal/mol, which is in agreement with Morokuma and co-workers' finding that the potential surface is very flat. The bending angle, θ, which is shown in Figures 2 and 3 is 46, 53, and 72° for **2a**, **3a**, and **5a**, respectively. The steric constraints of **2a**, **3a**, and **5a** can be used to explain the trend in θ.

The structures **2a**, **3a**, and **5a** exhibit some signs of an α-agostic interaction as revealed by $Zr-C_\alpha-H$ angles of less than 107°. This is in contrast to the RHF geometries of similar compounds[5a,b] with no signs of agostic interactions. However, it has been shown that the neglect of electron correlation in the Hartree–Fock method might underestimate the strength of agostic interactions.[21] Although the $Zr-C_\alpha-H$ angle is an adequate measure of the agostic distortion (as introduced by Morokuma and co-workers[5a,b]), we will be using the methyl tilt angle δ. The methyl group involved in the agostic interaction will exhibit a tilting, such that the C_3 axis of the methyl group no longer coincides with the M–C vector. The tilt angle δ is defined as the angle between the local C_3 axis and the M–C bond vector. Tilt angles for **2a**, **3a**, and **5a** are found to be 1, 20, and 30°, respectively (refer to Figures 2 and 3). We have attempted to estimate the strength of these interactions by performing single point energy calculations (no optimization) in which $\delta = 0°$, and comparing them to the corresponding fully optimized structures. This analysis reveals that 4 and 15 kJ/mol can be afforded to the agostic interactions in **3a** and **5a**, respectively. (No estimate for **2a** is given since it exhibits a negligible agostic distortion.) It should be noted that these energies represent the upper limit since only single point energies were determined.

The structure for the electrically neutral scandium analogue Cp_2Sc-CH_3, **4a**, compares well with the experimental X-ray structure determined by Thompson[22a] *et al.* The optimized $Sc-C_{Me}$ distance of 2.23 Å is in excellent agreement with the experimental distance of 2.24 Å. Other features of **4a** are in good agreement with experiment.[22a] Unlike its zirconium analogues, **4a** is not found in the bent sandwich configuration. Also, unlike its zirconium analogues, Cp_2Sc-CH_3 does not possess any α-agostic interactions. The lack of any agostic interaction in the neutral scandocene species is likely due to the less electron deficient Sc center.

Figure 4 provides atomic charges for **2a**, **3a**, **4a**, and **5a** based on a Mulliken population analysis. We note that the bis-Cp systems **2a** and **3a** have a positive charge on the zirconium atom of +2.39 and +2.46, respectively. It is thus clear that the introduction of a SiH_2 bridge has little influence on the charge of the central atom. For **5a** the positive charge on zirconium is reduced to 2.06, as the NH group is able to hold less of an electron charge than the Cp ligand. Finally, the charge on scandium of 1.89 in the electroneutral **4a** system is not very different from the zirconium charge in **5a**.

B. Ethylene Insertion. We shall now turn to a discussion of the insertion process described in eq 3. A comparison of the calculated insertion profiles for **2a**, **3a**, **4a**, and **5a** is shown in Figure 5A. The reaction coordinate R_{CC} in Figure 5 corresponds to the C_2-C_3 distance where C_2 and C_3 are defined in Figure 6. Large R_{CC} distances represent the free reactants, and R_{CC} decreases as the reaction progresses. In the calculations the reaction coordinate R_{CC} has been varied in steps while all other degrees of freedom were fully optimized within the symmetry constraint (if any) for each step. The starting structures for the linear transit calculations were essentially the free reactants where the R_{CC} distance was large. No symmetry constraint was used for **5a**, while for **2a**, **3a**, and **4a** a C_s symmetry constraint was imposed where the plane of symmetry passes through the Zr, C_1, C_2, and C_3 atoms, thus making the Cp rings equivalent to one another. Previous theoretical calculations[5a,b] of similar systems revealed that this is a reasonable constraint and that it has little effect on the results. It was further assumed that the inserting olefin formed an eclipsed structure, as shown in Figure 6A. This orientation of the methyl group allows for a strong M–H agostic interaction[5h] within the C_s plane. The staggered approach which is shown in Figure 6B was found to be less favorable.[5a,b] It was also assumed that the olefin approaches the metal–C_{Me} bond from the side of the open coordination site, as shown by path I of Figure 6A. Path II of Figure 6A was not explored but is expected to be unfavored. For the scandium complex **4a**, paths I and II are equivalent.

Ethylene Insertion into $Cp_2Zr-CH_3^+$: A Detailed Look. The reaction profile for insertion of ethylene into the unbridged zirconocene, **2a**, is shown in Figure 5B. Figure 7 displays the optimized geometries of the π-complex, **2b**, the approximate transition state, **2c**, and the direct product **2d**.

The π-complex, **2b**, was taken as the first minima along the reaction profile starting from the separate species **2a**

(21) (a) Weiss, H.; Haase, F.; Ahlrichs, R. *Chem. Phys. Lett.* **1992**, *194*, 492. (b) Endo, J.; Koga, N.; Morokuma, K. *Organometallics* **1993**, *12*, 2777.

(22) (a) Burger, B. J.; Thompson, M. E.; Cotter, W. D.; Bercaw, J. E. *J. Am. Chem. Soc.* **1990**, *112*, 1556. (b) Ziegler, T.; Folga, E.; Berces, A. *J. Am. Chem. Soc.* **1993**, *115*, 636.
(23) Piers, W. E.; Bercaw, J. F. *J. Am. Chem. Soc.* **1990**, *112*, 9406.
(24) (a) Deng, L.; Ziegler, T.; Fan, L. *J. Chem. Phys.* **1993**, *99*, 3823. (b) Fan, L.; Ziegler, T. *J. Am. Chem. Soc.* **1992**, *114*, 10890. (c) Deng, L.; Ziegler, T. *Int. J. Quantum Chem.*, in press.

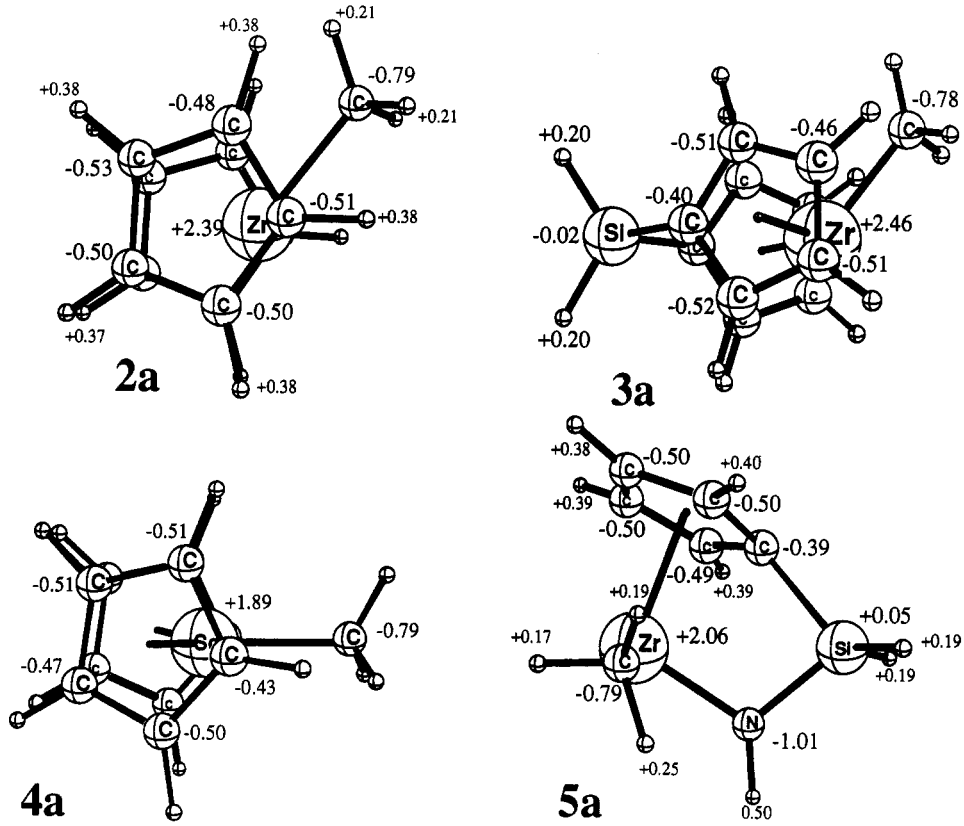

Figure 4. Mulliken population charges for **2a**, **3a**, **4a**, and **5a**.

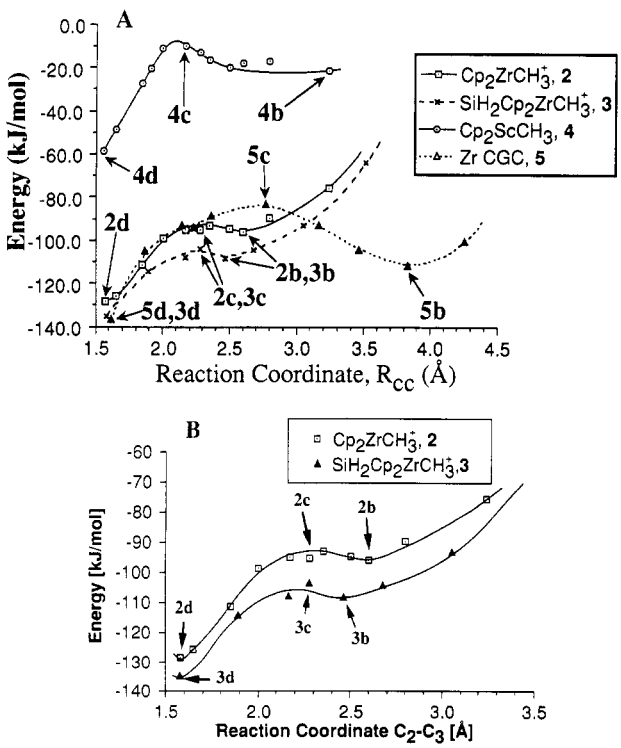

Figure 5. (A) Calculated energy profiles for the insertion process involving **2a**, **3a**, **4a**, and **5a**. The position of the π-complex is indicated by **nb**, the transition state by **nc** and the γ-agostic propyl product by **nd**. (B) Density functional energy profiles of the insertion process for zirconocenes **2** and **3** only.

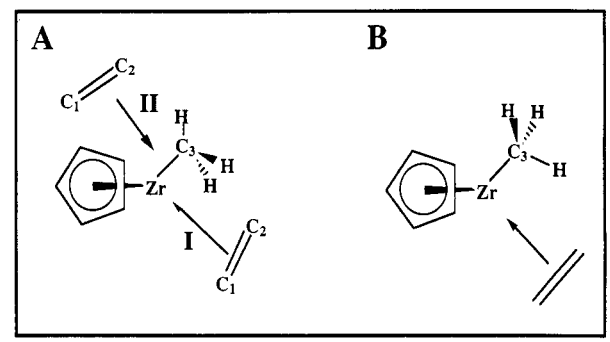

Figure 6. Olefin insertion pathways. (A) Path I illustrates the pathway that was modeled. This insertion forms eclipsed products. (B) The staggered insertion.

and C_2H_4. The potential well around **2b** is exceedingly shallow. The most striking feature of **2b** is the strong agostic interaction between the C_3–H bond and the zirconium atom. Methyl groups involved in agostic interactions exhibit a tilting, such that the C_3 axis of the methyl group no longer coincides with the M–C bond vector. The angle between the C_3 axis and the M–C bond vector, δ, is a measure of the distortion. The π-complexation of the olefin induces a methyl tilt of $\delta = 40.4°$. The small Zr–C_3–H angle of 74.6°, the short Zr–H distance of 2.20 Å, and the C_3–H distance of 1.15 Å are also evidence of the agostic interaction. In an attempt to estimate the strength of the agostic interaction in **2b** a single point energy calculation with $\delta = 0°$ was performed. **2b** with $\delta = 0°$ was found to be 31 kJ/mol less stable than the fully optimized structure. Here it is difficult to isolate the energy attributed strictly to the agostic interaction because the methyl tilt also allows for the interaction between C_2 and C_3. Another interesting feature of **2b** is the asymmetric π-olefin bond where Zr–C_1 = 2.50 Å and Zr–C_2 = 2.72 Å. An *ab initio* RHF structure[5b] of a comparable π-complex shows no strong agostic interaction and possesses a fairly symmetric π bond. As stated earlier, lack of an electron

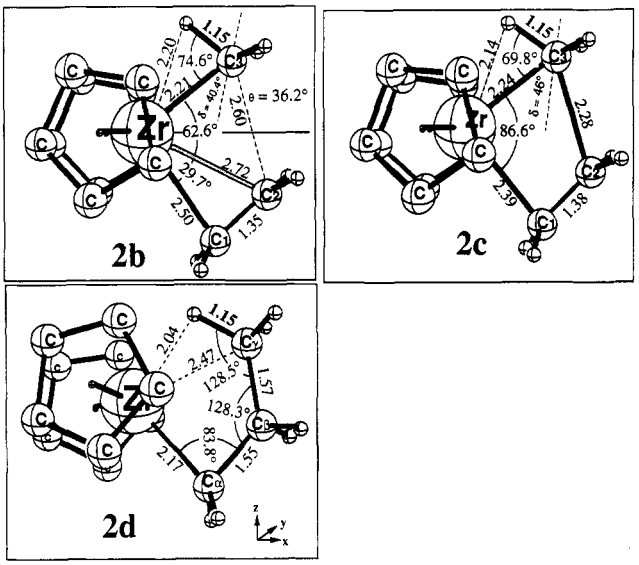

Figure 7. Optimized structures from the insertion of ethylene into zirconocene **2a**: (A) the π-complex, **2b**; (B) the transition state, **2c**; (C) the direct product, **2d**. The Cp ring hydrogens have been omitted for clarity.

correlation effect in the *ab initio* calculations depresses the influence of the agostic interaction. Another notable feature of **2b** is that the bent sandwich angle θ has decreased from 46° in **2a** to 36° in the π-complex.

It follows further from Figure 5B that the calculated π binding energy of ethylene to **2a** is 96 kJ/mol. The major part of the complexation energy comes from the stabilization of the electrons on C_2H_4 by the net positive charge on **2a**. The ethylene coordination is stabilized further by the olefin to metal donative bond. Metal to olefin back-bonding does not play any significant role due to the highly electron deficient nature of the d^0 metal center.

A transition state was initially searched for within C_s symmetry in an eclipsed conformation. However, no formal transition state could be found. The reaction path calculation, Figure 5, reveals that the barrier to insertion is only 3 kJ/mol, which is extremely small. This modest barrier and flat reaction profile provide an explanation for the failure to optimize the transition state.

The reaction path calculation provides an approximate transition state, **2c**, at a C_2–C_3 distance of 2.28 Å. The transition state occurs relatively early in the reaction. The C_1–C_2 double bond has only increased by 0.04 Å (3%) and the Zr–C_3 bond has increased by 0.06 Å (3%). Also the C_2–C_3 distance of 2.28 Å is much closer to the π-complex **2b** than the product **2d**. The agostic H–Zr interaction has increased from the π-complex. The methyl tilt has increased to 46° while the Zr–H distance and the Zr–C_3–H angle have decreased to 2.14 Å and 69.8°, respectively. It is obvious that the agostic interactions play an important role in stabilizing the transition state during the process. This is in agreement with recent experimental work by Piers[23] and theoretical work by Brintzinger and others.[5h]

The product of the insertion, a propylzirconium complex may assume several conformations of varying stability. The direct product of the insertion is an γ-agostic propyl structure, **2d**. Here C_3 becomes the γ carbon. **2d** has a short Zr–H_γ distance of 2.04 Å, suggesting a very strong agostic interaction. In addition to a donative interaction from the C_γ–H bond to Zr d_{xy} orbital, there is also a donative interaction from the C_α–C_β (C_1–C_2) bond to the same Zr d_{xz} orbital. The small Zr–C_α–C_β angle of 83.8° and the short Zr–C_β distance of 2.52 Å is suggestive of these agostic interactions. Although **2d** contains several stabilizing agostic interactions, all of its propyl hydrogens are in unfavorable eclipsing conformations.

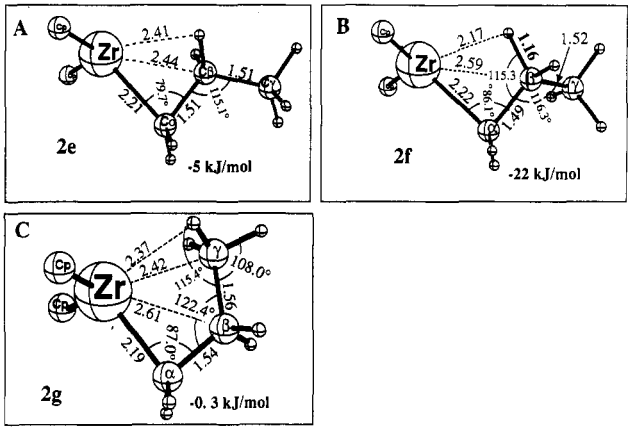

Figure 8. Optimized propyl structures: (A) all-staggered propyl in C_s symmetry, **2e**; (B) β-agostic propyl, **2f**; (C) the partially staggered γ-agostic propyl, **2f**. Values in parentheses reflect the energies relative to the direct product **2d**.

More stable conformations of the propyl product may be assumed after the insertion. Figure 8 shows several other stable conformations and their energies relative to **2d**. The structure **2e** which was optimized within C_s symmetry (and also with no symmetry constraints) can be described as an all-staggered C_s symmetry conformation. It is found to be 5 kJ/mol more stable than the γ-agostic product, **2d**. Although the eclipsing conformations are absent in this complex, the favorable agostic interactions are weakened. Structure **2f**, which was optimized with no symmetry constraints, is a β-agostic conformation. **2f** is the most stable conformation, being 22 kJ/mol lower in energy from **2d**. The stability can be attributed to the all-staggered orientation of the alkyl chain and the rather strong β-agostic interaction with the Zr–H_β distance optimized at 2.17 Å and the C_β–H bond length of 1.17 Å. By rotating the C_β–C_α bond in **2d** one arrives at conformation **2g**. This structure would be the direct product of an eclipsed insertion, as shown in Figure 6B. The conformation **2g** is slightly more stable than **2d**.

Ethylene Insertion into SiH_2Cp_2Zr–CH_3^+. The energy profile for the insertion of ethylene into the Zr–CH_3 bond of SiH_2Cp_2Zr–CH_3^+, **3a**, is shown in Figure 5A. Figure 5B provides a more detailed comparison of the insertion profiles involving the silane bridged species **3a** and the unbridged system **2a**. It follows from Figure 5B that the insertion profile for **3a** is more or less the same as the profile for **2a** except that it is more exothermic by about 12 kJ/mol. The monosilane bridge has two important effects. First, it opens up the coordination site of the complex by effectively "pulling back" the Cp rings, and secondly, it increases the charge deficiency of the Zr center, Figure 4. Pulling back the Cp rings is likely to reduce the steric repulsion during the reaction and thus increase the exothermicity of the insertion process.

As for the unbridged system **2a**, the π-complex involving **3a** is defined by a shallow energy minimum and the insertion is characterized by a low insertion barrier of 4 kJ/mol. It follows from Figure 9 that the π-complex, **3b**, the transition state, **3c**, and the direct product **3d**, are very similar in structure to the unbridged analogues, Figure

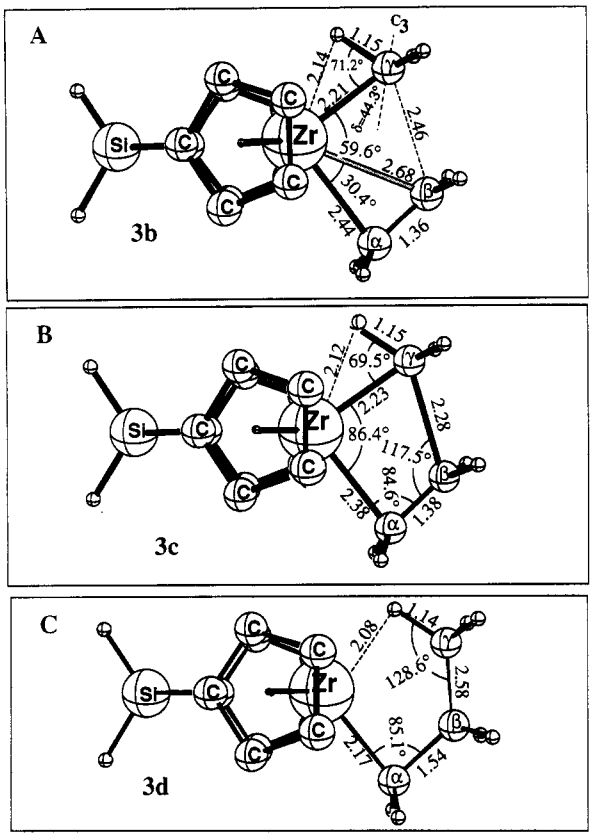

Figure 9. Optimized structures from the insertion of ethylene into the monosilane bridged zirconocene **3a**: (A) the π-complex, **3b**; (B) the transition state, **3c**; (C) the direct product, **3d**.

7. Other propyl structures analogous to **2e**, **2f**, and **2g** were not examined for the monosilane bridged zirconocene since they were expected to be very similar with regard to structure and relative energies. Our estimate of 4 kJ/mol for the insertion barrier involving **3a** is at variance with previous Hartree–Fock (HF) and MP2[5a] results in which the barrier involving **3a** was calculated to be 69.8 and 25.0 kJ/mol, respectively. Here the MP2 value was based on the HF geometry. Investigations have shown[24] that the present DF approach is of the same quality as MP4 calculations, and we expect that the ab initio barrier will be reduced at a higher level of *ab initio* theory.

Ethylene Insertion into Cp_2Sc-CH_3. The neutral d^0 scandocene **4a** is an isoelectronic homologue to the cationic species **2a**. It is interesting to note that the Sc–Cen distance of 2.17 Å in **4a** is quite similar to the Zr–Cen length of 2.19 Å in **2a**. Thus, the effective size of the neutral 3d element scandium is approximately the same as the size of the 4d cation, Zr^+. We shall in the following discuss how the replacement of the zirconium cation in **2a** and **3a** with a neutral scandium atom in **4a** will change the profile for the insertion process.

The insertion profile for **4a** is shown in Figure 5A. An obvious feature of the profile is that it is positioned roughly 80 kJ/mol above the profile for the insertion involving **2** and **3b**. The higher energy stems from the lack of the kind of ion–dipole interaction enjoyed by the cationic zirconium systems.

The π-complex **4b**, Figure 10, with a C_2-C_3 distance of 3.24 Å is only 20 kJ/mol more stable than the free reactants **4a** and C_2H_4. Also, the energy profile is very flat for a large region around **4b**. Arguably, any of the optimized

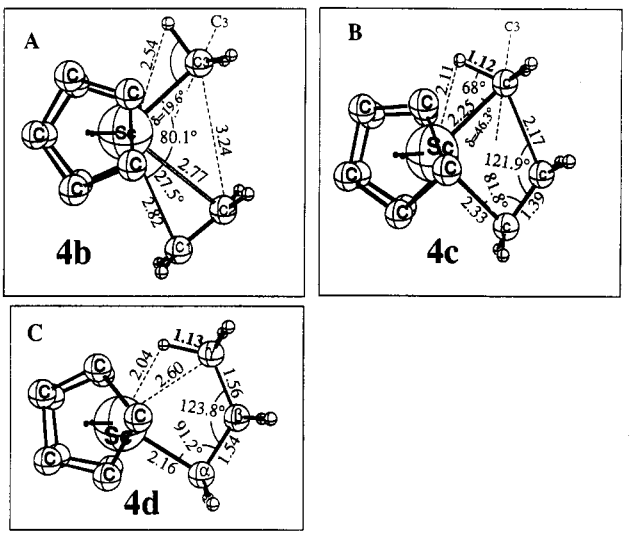

Figure 10. Optimized structures from the ethylene insertion into the unbridged scandocene **4a**: (A) π-complex, **4b**; (B) the transition state, **4c**; (C) the direct product, **4d**.

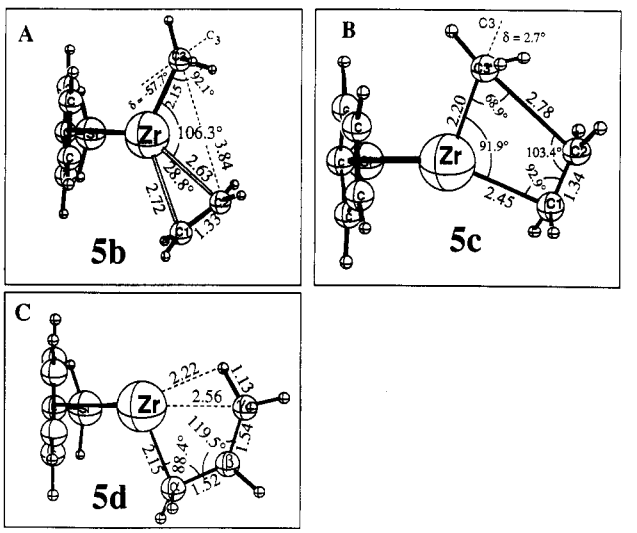

Figure 11. Optimized structures from the ethylene insertion into the zirconium constrained geometry catalyst **5a**: (A) π-complex, **5b**; (B) the transition state, **5c**; (C) the direct product, **5d**.

structures in the range C_2-C_3 = 2.50–3.50 Å could qualify as a π-complex. The olefin coordination in **4b** is very symmetric with the Sc–C_α and Sc–C_β distances being virtually equal. This is in contrast to the asymmetric Zr π-complex, **2b**, where Zr–C_α and Zr–C_β distances differ by more than 0.2 Å. Although the scandium π-complex is very weak, it still exhibits a significant agostic distortion where the C_3 axis of the methyl carbon is bent by $\delta = 20°$.

The transition state for the scandocene insertion **4c** of Figure 10, bears some resemblance to **2c**. It is a slightly more advanced transition state, as indicated by the longer C_1-C_2 bond of 1.39 Å and a shorter C_2-C_3 distance of 2.17 Å compared to C_1-C_2 = 1.38 and C_2-C_3 = 2.28 Å in **2c**. Also the α-agostic interaction is less pronounced with a C_α–H distance of 1.12 Å as compared to 1.15 Å for **2c**, Figure 7. The weaker α-agostic interaction can be explained by the fact that Sc is less electron deficient than Zr^+. The reduced α-agostic interaction might also be responsible for the fact that the calculated barrier of 14 kJ/mol for the insertion into **4a** is larger than the barriers of 3 and 4 kJ/mol found for **2a** and **3a**, respectively. The direct product **4d** is also

similar to its Zr counterpart **2d**. Another notable difference is that the M–C_α–C_β angle is 7° larger in the scanium complex (91 vs 84°). This is suggestive of a weaker agostic interaction between the C_α–C_β bond and the metal in **4d**.

Ethylene Insertion into the Zirconium Based Constrained Geometry Catalyst. The insertion profile for the mono Cp zirconium CGC, **5a**, is markedly different from those of the metallocenes. Figure 5A compares all of the insertion profiles. An obvious feature of the insertion profile for **5a** is that the complexation with the olefin begins at a much larger C_2–C_3 distances than for its bis-Cp Zr counterparts **2a** and **3a**. Unlike **2a** and **3a** a stable π-complex, **5b**, forms at a large C_2–C_3 value of 3.84 Å. The features of **5b** differ significantly from those of **2b**, **3b**, and **4b** in many other respects as well. Most notably, the angle between the methyl group and the π-olefin is much greater in the CGC. The C_3–Zr–C_2 angle is 106° in **5b** and roughly 60° in **2b** and **3b**. In a similar vein, the methyl group and the π-complexed olefin are noninteracting in the CGC, while the olefin in the bis-Cp systems induces a tilt of the methyl group. Tilt angles of δ = 40.4, 44.3, and 19.6° are observed in **2b**, **3b**, and **4b** respectively. This is in contrast to the CGC π-complex where the tilt is in the opposite direction and virtually unchanged from the uncoordinated complex **5a**. The agostic hydrogen of the methyl group is relatively unaffected by the complexation. The Zr–C_{Me}–H angle has increased marginally from 90 to 92°. Much like the scandocene complex, **4b**, the π-complex is very symmetric in **5b**. The π-complexation energy is 111.6 kJ/mol, much greater than in the zirconocenes **2b** and **3b** for the same R_{CC} distance. The more open coordination site of the CGC allows the olefin to form a less sterically congested π-complex, resulting in greater stabilization at large R_{CC} distances. Hoffmann and Lauher[5d] have predicted that the angle, θ, between the methyl fragment and the center of the olefin C–C bond that provides the greatest orbital overlap and stabilization is 110°. This is in good agreement with the θ angle of 120° in **5b**. The agostic interaction in **5b** may slightly increase the angle θ. For **2b** and **3b** θ is less than 90°.

The transition state, **5c**, which occurs at a linear transit distance of C_2–C_3 = 2.78 Å is 27 kJ/mol higher in energy than the π-complex, **5b**. Much like the bis-Cp transition states, **5c** occurs relatively early in the reaction. The C_1–C_2 double bond has stretched slightly to 1.34 Å and the Zr–C_3 bond has elongated by only 0.05 Å from the π-complex. Unlike the other transition states there is no H–Zr agostic stabilization. The methyl group has only tilted 2.7° from the "ideal" position. Also unlike the other transition states, the methyl group is partially staggered and the four centered transition state is not planar but twisted with the Zr–C_1–C_2–C_3 dihedral angle equal to 12.8°. One may argue that these features are absent in **2c**, **3c**, and **4c** because of the C_s symmetry constraint imposed, but a transition state optimization of **3c**[5b] with no symmetry constraints gives an eclipsed, planar complex in agreement with our results.

The direct product from the CGC insertion, **5d**, is also notably different from its bis-Cp counterparts. The product is partially staggered and nonplanar with a Zr–C_α–C_β–C_γ dihedral angle of 33.8°. Like its bis-Cp analogues, **5d** does posses an γ-agostic bond. The large Zr–H_γ distance of 2.22 Å is 0.2 Å greater than that observed in **2d** and reveals that the agostic bond is much weaker in the CGC. We note that formation of **5d** is slightly more exothermic than the formation of **2d**, Figure 5A. We attribute this to the more open coordination site around CGC which reduces the steric interaction between the propyl group and the other ligands around the metal center.

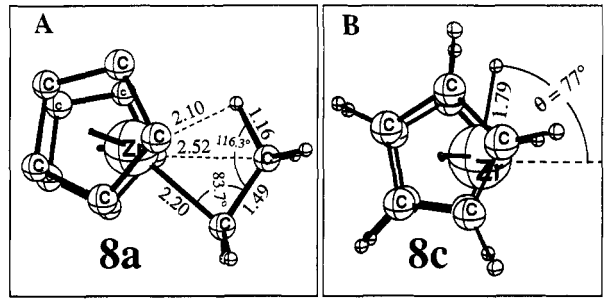

Figure 12. Optimized structures for the chain terminating β-hydride elimination: (A) the reactant **8a**; (B) the product **8c**.

IV. Chain Termination Processes

Two chain termination processes have been studied with density functional theory. For both processes, the unbridged zirconocene was used to model the catalyst.

A. β-Hydride Elimination. The proposed mechanism that was modeled for chain termination by β-hydride elimination is shown in eq 6. The reactant is an alkylzirconocene complex, **8a**, which has a β-agostic H–Zr

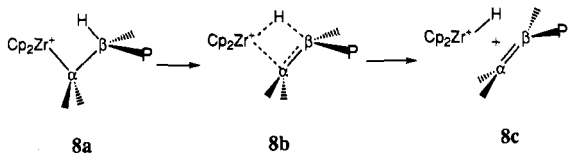

(6)

interaction similar to that of structure **2f**. The elimination process is thought to be initiated by the agostic interaction which, as it strengthens, passes through a four centered transition state, **8b**. This elimination process produces a vinyl terminated polymer chain and a zirconocene hydride complex, **8c**. Structures for the model reactant, **8a**, and the product **8c** have been optimized within a C_s symmetry constraint. These optimized structures are shown in Figure 12. Structure **8a** is analogous to the β-agostic propyl structure **2f**. Much like its propyl analogue, **8a** possesses a very strong β-agostic interaction, as evidenced by the short H_β–Zr bond of 2.10 Å. One of the products, a zirconocene hydride, **8c**, possesses a bent sandwich geometry much like the methylzirconocene, **2a**. Likely due to steric reasons, the bent sandwich angle θ is much larger in the hydride (θ = 77°) than in **2a** (θ = 46°).

The use of an ethyl group to model the growing chain in the β-hydride elimination reaction of eq 6 made it possible to take advantage of a preserved C_s symmetry throughout the reaction where the symmetry plane runs through the agostic H, Zr, C_α, and C_β. The postulated least motion pathway of eq 6 was assumed, and the H–C_β distance was used as the reaction coordinate in a reaction path calculation. The H–C_β distance was varied from 1.16 Å, the distance in the reactant, **8a**, to a distance of 10.6 Å, a distance where the products are essentially free. A total of six steps along the reaction profile were calculated by fixing the H–C_β distance and optimizing all other degrees of freedom within the C_s symmetry constraint. The calculated reaction profile is shown in Figure 13.

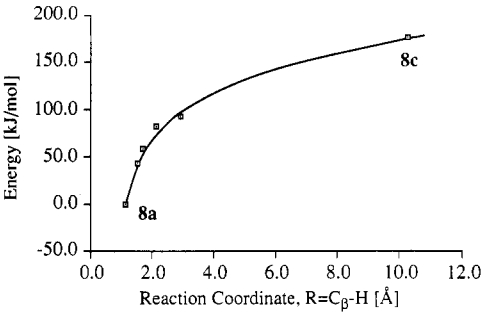

Figure 13. Calculated reaction profile for β-hydride elimination leading to chain termination. The C_β–H distance is the reaction coordinate. Small values for the reaction coordinate represent the reactants and large values represent the free products.

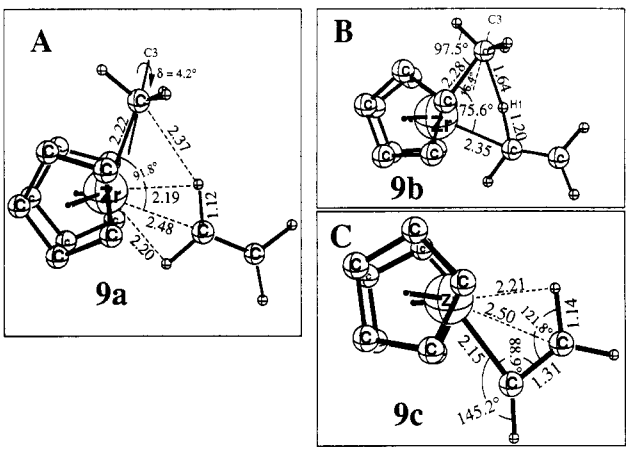

Figure 14. The optimized structures of **9a**, **9b**, and **9c**.

The reaction profile reveals that the process is endothermic by 176 kJ/mol and that the energy steadily increases during the course of the reaction until the products are formed. For this reason it is difficult to locate a transition state in this case. The reaction enthalpy of $\Delta H = 176$ kJ/mol is in agreement with other estimates for the β-hydride elimination enthalpy obtained experimentally from neutral scandocene complexes.[22a]

B. Alkene C–H Bond Activation by Cp_2Zr–CH_3^+. Another possible chain termination process that has been examined involves a vinylic C–H bond activation by the L_2M–R link. The proposed mechanism is shown in eq 7.

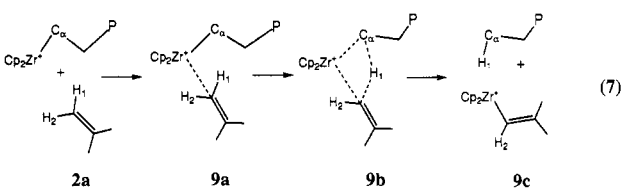

(7)

In this process the olefin molecule inserts into the M–R bond in a different orientation than that of the polymerization propagation. The first step of the reaction involves the formation of an ethylene adduct, **9a**. The adduct then passes through a four centered transition state, **9b**, in a σ bond metathesis reaction. The product of the reaction is an alkane terminated polymer chain and a vinyl–zirconocene, **9c**. DFT optimized structures of the model ethylene adduct, transition state, and vinyl-zirconocene are displayed in Figure 14.

The reaction profile for the C–H activation process is shown in Figure 15. The profile was determined by a

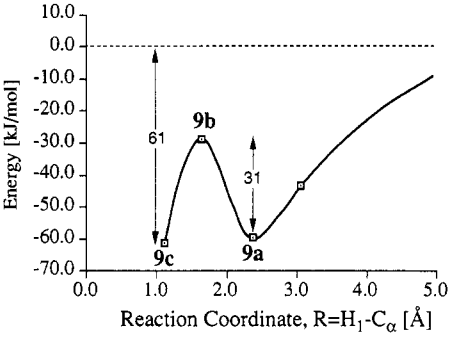

Figure 15. DFT reaction profile for the C–H activation chain termination process.

reaction path method similar to that described in previous sections for the β-hydride elimination and insertion processes. The postulated least motion pathway has a preserved C_s symmetry, which was maintained throughout the reaction. The H_1–C_α distance was used as a reaction coordinate and varied from 13 Å for the free reactants to a distance of 1.1 Å, the C–H distance in the methane product. As with previous calculations, all degrees of freedom were optimized within the symmetry constraint except for the reaction coordinate which was fixed.

The reaction profile reveals that the process is exothermic by 61 kJ/mol and is subject to a 31 kJ/mol electronic barrier. The transition state, **9b**, is 30 kJ/mol lower in energy than the reactants. Thus, from both a kinetic and thermodynamic viewpoint, this model indicates that chain termination by C–H activation is much more favored than that by β-hydride elimination. However alkene C–H bond activation is still less exothermic than ethylene insertion with a calculated reaction enthalpy of 129 kJ/mol, Figure 5B.

The ethylene adduct, **9a**, has a stability of 60 kJ/mol with respect to ethylene and **2a**. It is thus of higher energy than the π-complex **2b** for which the corresponding stability is 96 kJ/mol. However, unlike **2b** the ethylene adduct has a well-defined minima, Figure 15.

The ethylene molecule is complexed with the zirconocene through agostic interactions between the two vinylic C–H bonds and the Zr metal. Electrostatic interactions are also a source of stabilization in the adduct because of the electron deficiency of the metal center. No α-agostic interaction is observed with the methyl group tilting only slightly by 4.2°, which is in contrast to the tilt of 40.4° observed in the π-complex **2b**.

The four centered transition state, **9b**, occurs at a H_1–C_α distance of 1.64 Å in the linear transition calculation and is 31 kJ/mol higher in energy than the adduct. The large H_1–C_α distance at 1.64 Å shows that the transition state occurs relatively early in the reaction. Additionally, the vinylic C–H bond has elongated modestly to 1.20 Å from 1.12 Å in the adduct. A weak agostic interaction has formed, with the M–C_α–H angle decreasing to 97.5° and the methyl group tilting by 16.4°. The transition state is destabilized by the fact that the methyl carbon and the vinyl carbon both have σ orbitals which are unable to sustain optimal interactions with both the hydrogen which they are exchanging and the metal center.[22b]

The products of the model reaction are a vinyl–zirconocene, **9c**, and the methane molecule. The Zr–C_α bond distance of 2.15 Å in the vinyl complex is significantly shorter than in its ethyl counterpart **8a**, where it is 2.20 Å. The shortening of this bond is a result of the increased

role of the 2s orbital in the vinyl Zr–C bond. The small Zr–C_α–C_β angle of 88.9° and the short Zr–H distance of 2.21 Å in **9c** are suggestive of a strong β-agostic interaction. The presence of an agostic interaction is not surprising[22b] since we have found agostic interactions in all of the stable complexes we have studied. The bent sandwich angle θ is 51.8° as compared to 45° in the sp^3 methyl complex **2a**.

V. Concluding Remarks

We have investigated the ethylene insertion into the metal–methyl bonds of **2a**, **3a**, **4a**, and **5a**. The insertion process for the cationic zirconocenes is very favorable from a thermodynamic point of view. In the gas phase, our calculations show that the direct or kinetic products are approximately 130 kJ/mol more stable than the free reactants. The reaction enthalpy is reduced to $\Delta H = -60$ kJ/mol for the neutral scandocene catalyst, since the scandium system lacks the stabilizing ion–dipole interactions present in the zirconium species.

We have examined the insertion process for an unbridged zirconocene, **2a**, as well as a monosilane bridged species, **3a**. The effect of the bridge on the geometric and electronic structure of the zirconocenes is 2-fold. First it opens up the coordination site slightly by pulling back the Cp rings. The Cen–Zr–Cen angle is 139° in the unbridged species, **2a**, and 127° in the monosilane bridged species, **3a**. Secondly, by pulling back the Cp rings with the bridge the electron deficiency of the Zr center is increased; see the Mulliken populations in Figure 4. This is because the Cp ring orbitals cannot interact optimally with the Zr d orbitals. However, the effect of the monosilane bridge on the energetics of the insertion is very small, Figure 5B. The activation barrier is unchanged by the bridge, and the reaction enthalpy is increased slightly by 14 kJ/mol. The α-agostic interactions were found to be important[5h] throughout the insertion process for the bis-Cp catalysts **2a** and **3a** and in part responsible for the low insertion barrier of 3–4 kJ/mol found for **2a** and **3a**.

The profile for the scandocene **4a** is very similar to those of its Zr^+ counterparts **2a** and **3a**. However, the profile for **4a** is situated at higher energies due to the lack of stabilization from the type of ion–dipole interactions present in the cationic zirconium systems. Also, the insertion barrier of 14 kJ/mol for **4c** is calculated to be higher than those found for **2c** and **3c** of 3 and 4 kJ/mol, respectively. The scandium species has a weaker α-agostic interaction in the transition state than the zirconium systems since the neutral scandium is less electron deficient than the zirconium anion. The weaker α-agostic interaction might explain the higher barrier encountered for **4c**.

Although the constrained geometry catalyst has a more open coordination site, and potentially less steric hindrance to insertion, we find that the open nature of the catalyst actually increases the electronic barrier. The large coordination site of the CGC allows for the formation of a strong π-complex, **5b**, with a well-defined minimum at large C_2–C_3 distances of 3.90 Å (Figure 11). This is in contrast to the zirconocenes **2a** and **3a** where the π-interaction is weak at large C_2–C_3 distances. The ethylene molecule of **5b** has in part to abandon the π-interaction as it slides toward the methyl group in the last part of the insertion reaction. The result is an electronic barrier of 27 kJ/mol in **5c**. Although the large coordination site of the CGC increases the electronic barrier, we expect the more open site to better facilitate the insertion of larger, more sterically demanding comonomers.

It is difficult to assess experimental activity data for Kaminsky type metallocene systems.[25] It seems that **5a** and its Ti analogue are versatile copolymerization catalysts, but less active than **2a** and **3a** for ethylene polymerization.[25] This is in line with the profiles in Figure 5A. The scandium system **4a** should be quite active according to Figure 5A. However, it is found to be inactive due to dimerization of **4a**. The $Cp^*_2ScCH_3$ analogue of **4a** with $Cp^* = C_5(CH_3)_5$ does not dimerize, and it readily inserts ethylene.[26a] A scandium based CGC[26b] has also shown activity toward olefin polymerization.

Two chain termination processes have been modeled—β-hydride elimination and C–H activation. Hydrogenolysis is also an important chain terminating process; however, for metallocene based systems hydrogenolysis is too facile[22] and not often used to control molecular weights. For this reason we have not examined this process in detail for the Zr based systems. We have, however, determined that the process is exothermic by −44 kJ/mol where the polymer chain was modeled with a methyl group in $Cp_2ZrCH_3^+$.

Comparing β-hydride elimination and C–H activation we find that from both a kinetic and thermodynamic perspective, C–H activation is heavily favored as the prevailing chain terminating mechanism. Since β-hydride elimination is so thermodynamically unfavored with $\Delta H = 176$ kJ/mol it seems to be an unlikely chain termination mechanism. Speculation of termination by β-hydride elimination is spurred on by evidence of vinyl terminated polymer chains. However, chain termination by C–H activation which produces an alkane terminated chain and a vinylzirconocene can also account for vinyl terminated polymer chains. This is because the vinyl–zirconocene product is also an active species which can further polymerize olefin, yielding a vinyl terminated polymer. Additionally, other mechanisms for chain termination may account for vinyl terminated polymers. It is interesting to note here that recent studies of acid-catalyzed cracking of paraffinic hydrocarbons show that the long standing, generally accepted mechanism falls short when the thermodynamics of the process are considered.[27]

Acknowledgment. This investigation was supported by the Natural Sciences and Engineering Research Council of Canada (NSERC). We gratefully acknowledge the donors of the Petroleum Research Fund, administered by the American Chemical Society (ACS-PRF No. 27023-AC3). Dr. J. McMeeking and Dr. D. Harrison of NRTC are thanked for many useful discussions.

OM9307996

(25) Spaleck, W. Symposium on Ziegler Catalysts, Freiburg, Germany, 1993, private communication.

(26) (a) Burger, B. J.; Thompson, M. E.; Cotter, D.; Bercaw, J. E. *J. Am. Chem. Soc.* **1990**, *112*, 1566. (b) Shapiro, P. J.; Bunel, E. S.; Schaefer, W. P.; Bercaw, J. E. *Organometallics* **1990**, *9*, 867.

(27) (a) Sie, S. T. *Ind. Eng. Chem. Res.* **1992**, *31*, 1881. (b) Sie, S. T. *Ind. Eng. Chem. Res.* **1993**, *32*, 403. (c) Sie, S. T. *Ind. Eng. Chem. Res.* **1993**, *32*, 397.